SELF-ASSEMBLED MONOLAYERS AS HOLE SELECTIVE CONTACTS FOR PEROVSKITE SOLAR CELLS: EXPERIMENT VERSUS SIMULATIONS

[1,2]Meng-Hsueh KUO, [1]Naini JAIN, [1,2]Neda NEYKOVA, [1]Rupendra Kumar SHARMA, [3]Zhivko VELKOV, [4]Chih-Yu CHANG, [1]Jakub HOLOVSKÝ

[1]Centre for Advanced Photovoltaics, CTU in Prague, Faculty of Electrical Engineering, Prague, Czech Republic, EU

[2]Institute of Physics of the Czech Academy of Sciences, Prague, Czech Republic, EU

[3]Centre Faculty of Mathematics and Natural Sciences, South-West University "Neofit Rilski", Blagoevgrad, Bulgaria, EU

[4]Department of Materials Science and Engineering, National Taiwan University of Science and Technology, Taipei, Taiwan

https://doi.org/10.37904/nanocon.2024.4980

Abstract

Recent advances in the performance of perovskite solar cells (PSCs) have been strongly linked to advancements in interfacial engineering and the development of charge-selective contact. Self-assembled monolayers (SAMs) play an important role in inverted PSCs due to their distinctive and versatile ability to manipulate chemical and physical interface properties. Here we compared the dipole moments and energy levels of (2-(9H-carbazol-9-yl)ethyl)phosphonic acid (2PACz), (4-(3,6-Dimethyl-9H-carbazol-9-yl)butyl)phosphonic acid (Me-4PACz), (4-(3,6-Dimethoxy-9H-carbazol-9-yl)butyl)phosphonic acid (MeO-4PACz), and (2-(3,7-Dibromo-10H-phenothiazin-10-yl)ethyl)phosphonic acid (Br-2EPT) molecules and their impact on the energy conversion of PSC devices. Additionally, we simulated the dipole moment and surface charge effect device behavior to support our hypothesis. Finally, we observed that the fill factor behavior in both devices and simulations exhibited a similar trend, which correlated with the dipole moment of SAMs.

Keywords: Self-assembled monolayers, perovskite solar cells, dipole moment, surface charge, simulations

1. INTRODUCTION

Organic-inorganic hybrid metal halide perovskite solar cells have gained significant attention due to their exceptional optoelectronic properties, with the current power conversion efficiency (PCE) surpassing 26% [1,2]. Furthermore, the wide bandgap single-junction PSCs with a composition of $FA_{0.83}Cs_{0.17}Pb(I_{0.6}Br_{0.4})_3$ (1.72 eV) have achieved an efficiency of 19.4% [3], making them well-suited for application as the top cell in tandem solar cells [4]. In addition to engineering the perovskite compositions and controlling crystallization kinetics [5,6], the precise engineering of the interfaces between the perovskite absorber and contact interlayers is crucial for optimizing performance and stability [7]. Ultrathin self-assembled monolayers (SAMs) have recently been successfully employed as hole transport layers (HTLs) in inverted PSCs due to their ability to optimize interfacial properties [8], namely by improving energy level alignment [9], reducing recombination losses [10], enhancing stability [11], and increasing overall device efficiency [11]. The SAMs offer molecular-level control over interface engineering by introducing a permanent dipole moment, which can improve charge transfer across the interface through energy level alignment [7]. Moreover, fixed charges in SAMs can effectively passivate surface traps, minimizing non-radiative recombination and enhancing charge extraction [12]. The combination of dipole moments and fixed charges significantly reduces the energy barriers in the interface,

optimizing the local electric field and enhancing charge transport. This leads to a notable improvement in the PCE and long-term stability of the device [13].

Herein, we report the comparison of four carbazole-based SAMs with various dipole moments, highest occupied molecular orbital (HOMO), and lowest occupied molecular orbital (LUMO) energy levels for application in inverted PSCs. As the absorber for PSCs, we chose wide bandgap material with composition $FA_{0.83}Cs_{0.17}Pb(I_{0.6}Br_{0.4})_3$. Furthermore, we also simulated using various tunneling models, including band-to-band tunneling, quantum tunneling, thermionic tunneling, trap-assisted tunneling, and universal Schottky tunneling, to compare our experimental findings more efficiently. Our combined experimental and simulation results demonstrate that SAMs with higher dipole moments lead to improved fill factors in inverted PSCs, while the correlation of device performance with HOMO and LUMO energies was not confirmed.

2. METHODS

1.1 Perovskite films and solar cell fabrication

$FA_{0.83}Cs_{0.17}Pb(I_{0.6}Br_{0.4})_3$ perovskite films were prepared by dissolving 0.83 mmol of FAI, 0.17 mmol of CsI, 0.4 mmol of PbI_2, and 0.6 mmol of $PbBr_2$ in 1 ml of a DMF and DMSO solvent mixture at a 4:1 ratio. The precursor solution was stirred continuously at 70°C. The solution was then deposited onto the substrate via spin-coating, starting at 1000 rpm for 10 seconds, followed by 5000 rpm for 30 seconds. Five seconds before completing the second spin-coating step, 150 µL of chlorobenzene was applied to the substrate. The samples were subsequently annealed at 100°C for 30 minutes. All procedures were conducted in a nitrogen-filled glovebox.

The ITO-coated glass substrates (10 ohm/sq) were washed by ultrasonic cleaning in a 2% Hellmanex detergent solution, followed by rinsing with deionized water, acetone, and ethanol for 15 minutes each. After drying the substrates using a nitrogen gas gun, they were cleaned with a UV-ozone cleaner for 15 minutes. The single-junction cells structure is ITO/SAMs/$FA_{0.83}Cs_{0.17}Pb(I_{0.6}Br_{0.4})_3$/$PC_{61}BM$/BCP/Ag, where different SAMs materials are used: 2PACz, Me-4PACz: PFN-Br (9.5:0.5), MeO-4PACz, or Br-2EPT. The concentration of 2PACz, MeO-4PACz, and Br-2EPT solution were 1 mmol/l in ethanol. To prepare Me-4PACz:PFN-Br solution, both Me-4PACz and PFN-Br were dissolved in methanol at 0.4 mg/ml each. The SAMs were deposited using spin-coating at 4000 rpm for 30 seconds, followed by annealing at 100 °C for 10 minutes. After cooling down, the SAMs were dynamically washed with ethanol at 4000 rpm for 30 seconds and subsequently annealed again at 100 °C for 3 minutes. Next, the perovskite layer deposited onto SAM fabrication as described above. $PC_{61}BM$ at a concentration of 20 mg/mL in chlorobenzene, was then spin-coated onto perovskite layer at 2000 rpm for 30 seconds, followed by BCP, at a concentration of 0.5 mg/mL in IPA, was spin-coated at 5000 rpm for 30 seconds. Finally, an 80 nm Ag back contact was thermally evaporated onto the BCP layer under high vacuum using a shadow mask, with each electrode having an active area of 0.09 cm^2.

1.2 Device characterizations

Current density-voltage (*J-V*) characterization. The *J-V* measurements were carried out with a Keithley 2400 source meter managed by a computer, under a 100 mW/cm^2 illumination. The illumination was provided by a calibrated solar simulator (Wavelabs) giving AM 1.5 spectrum.

External quantum efficiency (EQE). The EQE measurements were conducted using a Bentham TMC 300 monochromator, a 50 W tungsten halogen lamp, SR570 preamplifier, NI DAQ A-D convertor and a software lock-in analyser.

Photoluminescence (PL). The PL intensity spectra were measured using a fluorescence spectrophotometer (Cary Eclipse) with a 300 nm excitation wavelength.

Scanning electron microscopy (SEM). The SEM measurements were carried out to determine the thickness of the perovskite thin films by examining the sample cross sections using the MAIA 3 scanning electron microscope from TESCAN at a voltage of 5 kV.

All measurements were conducted in an ambient atmosphere at room temperature without encapsulation.

1.3 Simulation

The simulated PSCs include ITO/SAMs/Perovskite/PCBM/BCP/Ag stacks on 400 nm thick $FA_{0.83}Cs_{0.17}Pb(I_{0.6}Br_{0.4})_3$ perovskite absorber, with ambipolar doping (10^{14} cm^{-3}), band gap (1.75 eV), and affinity (4.0 eV). The front and rear contact consists of ITO/SAMs and BCP/Ag interfaces, with a work function of approximately 5.1 eV and 4.0 eV. The DFT calculated parameters for SAM molecules were used in TCAD simulations for analysing the SAMs dipole moment effects on the performance of PSCs.

1.4 Density Functional Theory Calculations

To determine the values of dipole moment and HOMO, LUMO energies Density Functional Theory (DFT) calculations were performed. The calculations of dipole moments were carried out using the DFT [14], as implemented in the Gaussian09 program package. The optimization of the geometry was performed with the Becke 3-parameter hybrid exchange functional combined with the Lee et al. correlation functional (B3LYP) [15,16] with the standard double-ζ 6-31G(d,p) basis set [17]. The optimization was achieved without any geometry constraints. All possible intramolecular interactions were taken into account in the initial geometries. For all structures, the harmonic vibrational frequencies were computed to confirm the true minima on the calculated potential surface.

2. RESULT AND DISSCUSSION

Figure 1 (**a**) presents the molecular structure of the compounds used in this study: 2PACz, Me-4PACz, MeO-4PACz, and Br-2EPT. We considered 2PACz as a reference due to its extensive study in p-i-n structured PSC using SAMs. To understand the device behaviour with energy level alignment and charge dynamics, we first calculate the dipole moment, E_{HOMO}, and E_{LUMO} parameters for each SAM. As shown in **Table 1**, MeO-4PACz and Br-2EPT exhibit higher dipole moments compared to 2PACz and Me-4PACz, with values exceeding 3.5 debye. Notably, under certain conditions, a higher dipole moment can enhance the efficiency of perovskite solar cells by improving charge separation, reducing recombination, and optimizing energy band alignment. **Figure 1** (**b**) presents a schematic of the band edge positions for the SAMs and perovskite. Proper alignment of the band edges, along with a moderate amount of fixed charge at the interface, can facilitate the separation of photo-generated electron-hole pairs. This separation is driven by an electric field, which directs charges in opposite directions, thereby minimizing recombination and enhancing the efficiency of solar cells.

Table 1 Dipole moment, E_{HOMO}, and E_{LUMO} parameters of SAMs

SAMs	Dipole moment (Debye)	E_{HOMO} (eV)	E_{LUMO} (eV)
2PACz	1.94	-5.44	-0.75
Me-4PACz	1.65	-5.15	-0.60
MeO-4PACz	3.61	-4.98	-0.76
Br-2EPT	3.78	-5.32	-1.02

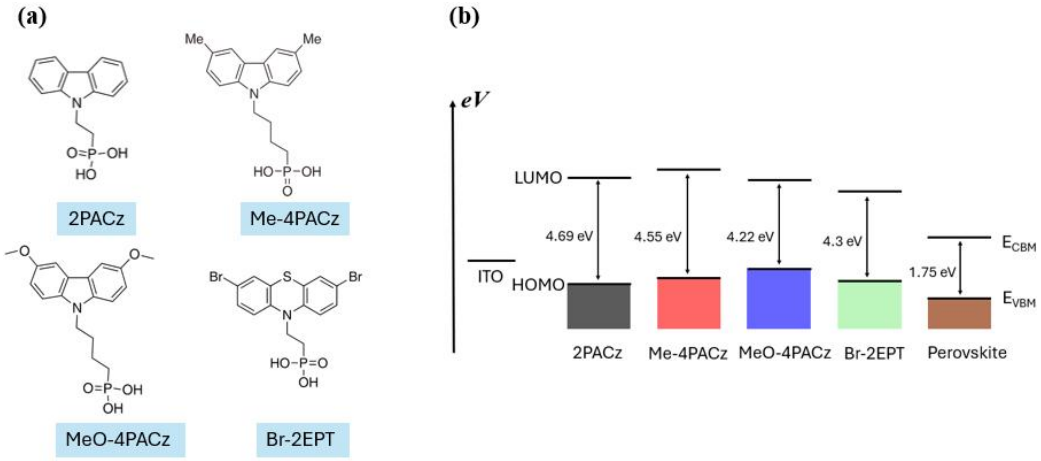

Figure 1 (a) Molecule structure of SAMs and (b) schematic of the band edge positions for the ITO, SAMs, and perovskite

To understand the effects of dipole moments and surface charges in solar devices, we fabricated four p-i-n SAMs PSCs (**Figure 2 (a)**) and analyzed their optical performance. Notably, Me-4PACz poses a hydrophobicity challenge during perovskite formation. To address this issue and enhance the quality of the perovskite film, we mixed Me-4PACz with PFN-Br in a ratio of 9.5:0.5 [18]. In **Figure 2 (b)**, the PL spectra of perovskite on various glass/SAM substrates are presented. The PL peak intensity at approximately 698 nm is slightly lower in the higher dipole moment MeO-4PACz and Br-2EPT samples, demonstrating more efficient charge extraction, compared to the 2PACz and Me-4PACz samples exhibiting lower charge extraction efficiency. This behavior of SMAs refers to the ability to passivate the surface. **Figure 2 (c)** shows the cross-sectional SEM image of the PSC, the SAM is not discernible, potentially due to the tunneling effect. **Table 2** summarizes the Voc, Jsc, FF, and PCE recorded for each of the best-performing cells. In these wide-bandgap PSCs, the Voc exceeded 1.1 V, which is suitable for tandem solar cell applications. Furthermore, the PSC based on MeO-4PACz achieved the highest efficiency of 13%.

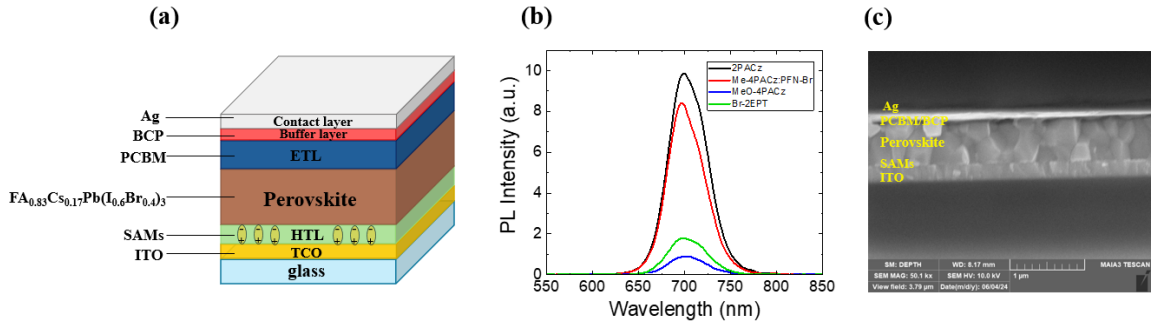

Figure 2 (a) Device architecture of this study; (b) Photoluminescence (PL) spectra; (c) Cross-sectional image for the PSC

Table 2 Summary of photovoltaic parameters extracted from the J−V measurements of best-performing PSCs with different SAMs

SAMs	V_{OC} (V)	J_{SC} (mA*cm^{-2})	FF (%)	PCE (%)
2PACz	1.17	14.29	67.0	11.23
Me-4PACz:PFN-Br	1.13	12.42	68.8	9.66
MeO-4PACz	1.16	14.78	77.1	13.16
Br-2EPT	1.12	13.56	75.7	11.48

Figure 3 (a) presents the distribution of photovoltaic parameters for both forward and reverse scans. We compared the device behaviour with the dipole moment and energy levels of the SAMs. Notably, the fill factor graph reveals a trend that corresponds to the dipole moment of the SAMs.

We conducted simulations to investigate the effect of varying interface charges on the dipole moment of SAMs in PSCs. For this investigation, we varied the dipole moment by varying the interface charge density (σ) and separation distance (x) while ensuring the dipole moment remains constant, as determined by DFT simulations.

Figure 3 (b) illustrates the simulation results for the fill factor at the ITO/SAMs interface for the calculated distance and surface charge density (i.e. x = 2 nm, and σ= 2 ~ 5 × 10^{11}), analysed for different SAMs. The results show consistent trends with varying dipole moments and interface charges.

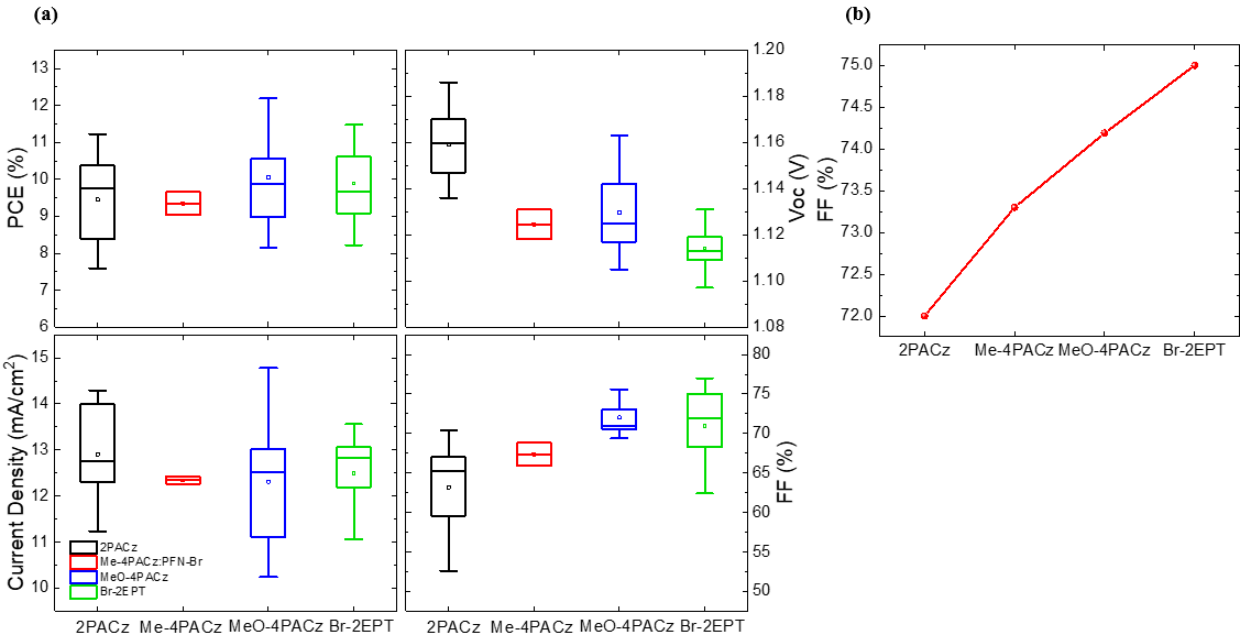

Figure 3 (a) Boxplots of PSCs optical parameters; (b) The simulated fill factor for 2 nm distance in surface charges for the dipole moment.

3. CONCLUSION

This study has analysed the effect of dipole moment and energy level parameters of 2PACz, Me-4PACz, MeO-4PACz, and Br-2EPT, on their electrical performance in inverted PSCs. This was accompanied by DFT and electronic simulations. A clear correlation between dipole moment and fill factor was consistently observed between experimental data and simulation results. These findings underscore the critical role of dipole moment in SAMs for enhancing carrier transport efficiency and suppressing interfacial recombination in PSC devices.

ACKNOWLEDGEMENTS

We acknowledge the support of Czech Science Foundation through grant no 23-06543S and the support of Czech Technical University in Prague and National Taiwan University of Science and Technology through joint Collaborative Research Project CTU-NTUST.

REFERENCES

[1] PARK, J.; KIM, J.; YUN, H.-S.; PAIK, M.J.; NOH, E.; MUN, H.J.; KIM, M.G.; SHIN, T.J.; SEOK, S.I. Controlled Growth of Perovskite Layers with Volatile Alkylammonium Chlorides. *Nature.* 2023, vol. 616, pp. 724–730, Available from: https://doi.org/10.1038/s41586-023-05825-y.

[2] CHEN, H.; LIU, C.; XU, J.; MAXWELL, A.; ZHOU, W.; YANG, Y.; ZHOU, Q.; BATI, A.S.R.; WAN, H.; WANG, Z.; et al. Improved Charge Extraction in Inverted Perovskite Solar Cells with Dual-Site-Binding Ligands. *Science.* 2024, vol. 384, pp. 189–193. Available from: https://doi.org/10.1126/science.adm9474.

[3] GHARIBZADEH, S.; ABDOLLAHI NEJAND, B.; JAKOBY, M.; ABZIEHER, T.; HAUSCHILD, D.; MOGHADAMZADEH, S.; SCHWENZER, J.A.; BRENNER, P.; SCHMAGER, R.; HAGHIGHIRAD, A.A.; et al. Record Open-Circuit Voltage Wide-Bandgap Perovskite Solar Cells Utilizing 2D/3D Perovskite Heterostructure. *Advanced Energy Materials.* 2019, vol. 9, 1803699. Available from: https://doi.org/10.1002/aenm.201803699.

[4] KUMAR, A.; KUMAR, D.; JAIN, N.; KUMAR, M.; GHODAKE, G.; KUMAR, S.; SHARMA, R.K.; HOLOVSKY, J.; SAJI, V.S.; SHARMA, S.K. Enhanced Efficiency and Stability of Electron Transport Layer in Perovskite Tandem Solar Cells: Challenges and Future Perspectives. *Solar Energy.* 2023, vol. 266, 112185. Available from: https://doi.org/10.1016/j.solener.2023.112185.

[5] JEON, N.J.; NOH, J.H.; YANG, W.S.; KIM, Y.C.; RYU, S.; SEO, J.; SEOK, S.I. Compositional Engineering of Perovskite Materials for High-Performance Solar Cells. *Nature.* 2015, vol. 517, pp. 476–480. Available from: https://doi.org/10.1038/nature14133.

[6] CHEN, Y.; LI, N.; WANG, L.; LI, L.; XU, Z.; JIAO, H.; LIU, P.; ZHU, C.; ZAI, H.; SUN, M.; et al. Impacts of Alkaline on the Defects Property and Crystallization Kinetics in Perovskite Solar Cells. *Nat Commun.* 2019, vol. 10, 1112. Available from: https://doi.org/10.1038/s41467-019-09093-1.

[7] WANG, J.; BI, L.; HUANG, X.; FENG, Q.; LIU, M.; CHEN, M.; AN, Y.; JIANG, W.; LIN, F.R.; FU, Q.; et al. Bilayer Interface Engineering through 2D/3D Perovskite and Surface Dipole for Inverted Perovskite Solar Modules. *eScience.* 2024, 100308. Available from: https://doi.org/10.1016/j.esci.2024.100308.

[8] KIM, S.Y.; CHO, S.J.; BYEON, S.E.; HE, X.; YOON, H.J. Self-Assembled Monolayers as Interface Engineering Nanomaterials in Perovskite Solar Cells. *Advanced Energy Materials.* 2020, vol. 10, 2002606. Available from: https://doi.org/10.1002/aenm.202002606.

[9] KAHN, A.; KOCH, N.; GAO, W. Electronic Structure and Electrical Properties of Interfaces between Metals and Π-conjugated Molecular Films. *J Polym Sci B Polym Phys.* 2003, vol. 41, pp. 2529–2548. Available from: https://doi.org/10.1002/polb.10642.

[10] DENG, X.; QI, F.; LI, F.; WU, S.; LIN, F.R.; ZHANG, Z.; GUAN, Z.; YANG, Z.; LEE, C.; JEN, A.K. -Y. Co-assembled Monolayers as Hole-Selective Contact for High-Performance Inverted Perovskite Solar Cells with Optimized Recombination Loss and Long-Term Stability. *Angewandte Chemie.* 2022, vol. 134, e202203088. Available from: https://doi.org/10.1002/ange.202203088.

[11] ALI, F.; ROLDÁN-CARMONA, C.; SOHAIL, M.; NAZEERUDDIN, M.K. Applications of Self-Assembled Monolayers for Perovskite Solar Cells Interface Engineering to Address Efficiency and Stability. *Advanced Energy Materials.* 2020, vol. 10, 2002989. Available from: https://doi.org/10.1002/aenm.202002989.

[12] YANG, Y.; CHENG, S.; ZHU, X.; LI, S.; ZHENG, Z.; ZHAO, K.; JI, L.; LI, R.; LIU, Y.; LIU, C.; et al. Inverted Perovskite Solar Cells with over 2,000 h Operational Stability at 85 °C Using Fixed Charge Passivation. *Nat Energy.* 2023, vol. 9, pp. 37–46. Available from: https://doi.org/10.1038/s41560-023-01377-7.

[13] MA, Y.; GONG, J.; ZENG, P.; LIU, M. Recent Progress in Interfacial Dipole Engineering for Perovskite Solar Cells. *Nano-Micro Lett.* 2023, vol. 15, 173. Available from: https://doi.org/10.1007/s40820-023-01131-4.

[14] KOHN, W.; BECKE, A.D.; PARR, R.G. Density Functional Theory of Electronic Structure. *J. Phys. Chem.* 1996, vol. 100, pp. 12974–12980. Available from: https://doi.org/10.1021/jp960669l.

[15] BECKE, A.D. Density-Functional Exchange-Energy Approximation with Correct Asymptotic Behavior. *Phys. Rev. A.* 1988, vol. 38, pp. 3098–3100. Available from: https://doi.org/10.1103/PhysRevA.38.3098.

[16] LEE, C.; YANG, W.; PARR, R.G. Development of the Colle-Salvetti Correlation-Energy Formula into a Functional of the Electron Density. *Phys. Rev. B.* 1988, vol. 37, pp. 785–789. Available from: https://doi.org/10.1103/PhysRevB.37.785.

[17] PARR, R.G. Density Functional Theory of Atoms and Molecules. In *Horizons of Quantum Chemistry*; Fukui, K., Pullman, B., Eds.; Springer Netherlands: Dordrecht, 1980; pp. 5–15. ISBN 978-94-009-9029-6.

[18] HOSSAIN, K.; KULKARNI, A.; BOTHRA, U.; KLINGEBIEL, B.; KIRCHARTZ, T.; SALIBA, M.; KABRA, D. Resolving the Hydrophobicity of the Me-4PACz Hole Transport Layer for Inverted Perovskite Solar Cells with Efficiency >20%. *ACS Energy Lett.* 2023, vol. 8, pp. 3860–3867. Available from: https://doi.org/10.1021/acsenergylett.3c01385.